JOURNAL OF AGRICULTURAL AND FOOD CHEMISTRY

Agricultural and Environmental Chemistry

Discovery of Novel Pyrazole-Quinazoline-2,4-dione Hybrids as 4-Hydroxyphenylpyruvate Dioxygenase Inhibitors

Bo He, Feng-Xu Wu, Liang-Kun Yu, Lei Wu, Qiong Chen, Ge-Fei Hao, Wen-Chao Yang, Hong-Yan Lin, and Guang-Fu Yang

J. Agric. Food Chem., **Just Accepted Manuscript** • DOI: 10.1021/acs.jafc.0c00051 • Publication Date (Web): 14 Apr 2020

Just Accepted

is published by the American Chemical Society. 1155 Sixteenth Street N.W., Washington, DC 20036

Discovery of Novel Pyrazole−Quinazoline-2,4-dione Hybrids as 4-Hydroxyphenylpyruvate Dioxygenase Inhibitors

Bo He,[†] Feng-Xu Wu,[†] Liang-Kun Yu,[†] Lei Wu,[†] Qiong Chen,[†] Ge-Fei Hao,[†] Wen-Chao Yang,[†] Hong-Yan Lin,[†, *] Guang-Fu Yang[†, #, *]

[†]Key Laboratory of Pesticide & Chemical Biology of Ministry of Education, International Joint Research Center for Intelligent Biosensor Technology and Health, College of Chemistry, Central China Normal University, Wuhan 430079, P.R. China

[#]Collaborative Innovation Center of Chemical Science and Engineering, Nankai University, Tianjin 300071, P.R. China

AUTHOR INFORMATION

Corresponding Authors:

[*]Tel: +86-27-67867800. Fax: +86-27-67867141. E-mail: gfyang@mail.ccnu.edu.cn

[*]Hong-Yan Lin, E-mail: 913975503@qq.com

ORCID:

Hong-Yan Lin: 0000-0002-5627-3708

Ge-Fei Hao: 0000-0003-4090-8411

Guang-Fu Yang: 0000-0003-4384-2593

ABSTRACT:

4-Hydroxyphenylpyruvate dioxygenase (HPPD, EC 1.13.11.27) has been identified as one of the most significant targets in herbicide discovery for resistant weed control. In a continuing effort to discover potent novel HPPD inhibitors, we adopted a ring−expansion strategy to design a series of novel pyrazole−quinazoline-2,4-dione hybrids based on the previously discovered pyrazole−isoindoline-1,3-dione scaffold. One compound, 3-(2-chloro-phenyl)-6-(5-hydroxy-1,3-dimethyl-1H-pyrazole-4-carbonyl)-1,5-dimethylquinazoline-2,4(1H, 3H)-dione (**9bj)**, displayed excellent potency against *At*HPPD with an IC_{50} value of 84 nM, which is approximately 16-fold more potent than pyrasulfotole (IC_{50} = 1359 nM) and 2.7-fold more potent than mesotrione (IC_{50} = 226 nM). Furthermore, the co-crystal structure of the *At*HPPD−**9bj** complex (PDB ID: 6LGT) was determined at a resolution of 1.75 Å. Similar to the existing HPPD inhibitors, **9bj** formed a bidentate chelating interaction with the metal ion and a π-π stacking interaction with Phe381 and Phe424. In contrast, the *o*-chlorophenyl at the N3 position of quinazoline-2,4-dione with a double conformation was surrounded by hydrophobic residues (Met335, Leu368, Leu427, Phe424, Phe392, and Phe381). Remarkably, the greenhouse assay indicated that most compounds displayed excellent herbicidal activity (complete inhibition) against at least one of the tested weeds at the application rate of 150 g ai/ha. Most promisingly, compounds **9aj** and **9bi** not only exhibited prominent weed control effects with a broad spectrum, but also showed very good crop safety to cotton, peanuts and corn at the dose of 150 g ai/ha.

KEYWORDS: 4-hydroxyphenylpyruvate dioxygenase, quinazoline-2,4-dione, structure−activity relationship, herbicidal activity

46 **INTRODUCTION**

47 It is well known that crops compete with weeds for water, nutrients, light, and space
48 during their whole growth process, so herbicides will continue to play an irreplaceable role in
49 modern agricultural production.[1, 2] 4-Hydroxyphenylpyruvate dioxygenase (HPPD, EC
50 1.13.11.27) is a non-heam iron-dependent oxygenase that exists in most aerobic organisms.[3, 4]
51 In most aerobic forms of life, it catalyzes the second reaction in the catabolism of tyrosine
52 which is the conversion of *p*-hydroxyphenylpyruvic acid (HPPA) into homogentisic acid
53 (HGA).[5, 6] In plants, HGA can be further transformed into two isoprenoids, plastoquinone and
54 tocopherol, which are both essential cofactors in photosynthesis.[7-12] The inhibition of HPPD
55 results in the blockage of natural tyrosine physiological metabolism, which in turn results in the
56 obstruction of photosynthesis in plants and plant death with bleaching symptoms.[13-17]

57 The first-generation pyrazole-type HPPD inhibitors, such as pyrazolinate, pyrazoxyfen and
58 benzofenap (**Figure 1**), were mainly used to control weeds in the rice fields with application
59 rates up to 4 kg ai/ha.[18, 19] After HPPD was identified as the action target of these herbicides,
60 structure-based discovery of novel HPPD inhibitors has become a hot area for pesticide
61 chemists worldwide and has produced second-generation pyrazole-type HPPD inhibitors with
62 significantly reduced application rates, including topramezone, pyrasulfotole, and
63 tolpyralate.[20-23] However, these products are mainly used for the weed control of corn and
64 cereal fields, and new HPPD-inhibiting herbicides for other crops are of great urgency due to
65 the rapid development of weed resistance.[24]

66 Previously, we reported that the pyrazole-isoindoline-1,3-dione hybrid is a promising
67 scaffold for developing HPPD inhibitors.[25] From the co-crystal structure of the

68 inhibitor−*At*HPPD complex (PDB ID: 6JX9, **Figure 2**), we could clearly observe that, apart
69 from the bidentate chelating interaction with the metal ion, the π−π stacking between the
70 isoindoline-1,3-dione moiety and the surrounding aromatic residues (Phe381 and Phe424)
71 contributed significantly to the binding. It has been reported that improving the π−π interaction
72 between inhibitors and their surrounding residues is an effective way to design new inhibitors
73 with improved potency.[26, 27] Therefore, we designed a quinazoline-2,4-dione scaffold (**Figure 2**)
74 by inserting a nitrogen atom between the benzene ring and the carbonyl of
75 isoindoline-1,3-dione *via* a ring−expansion strategy. We expected that the six−membered
76 heterocyclic ring would improve the π−π interaction. Computational simulation results
77 indicated that the quinazoline-2,4-dione moiety was surrounded by hydrophobic residues
78 (Met335, Leu427, and Leu368). The binding free energy of the designed new molecule (**9aa**,
79 **Figure 2**) is -8.349 kcal/mol, which is significantly better than that of the corresponding
80 pyrazole−isoindoline-1,3-dione derivative (**s1**, ΔH_{S1} = -6.322 kcal/mol). Herein, we report the
81 design, syntheses, inhibitors effect against *At*HPPD, structure−activity relationships, and
82 herbicidal activity. In addition, we resolved the co-crystal structure of *At*HPPD in complex with
83 the representative title compound at a resolution of 1.75 Å.
84

85 **MATERIALS AND METHODS**

86 **Chemicals and Instruments.** During the experiment, all the solvents were either
87 chemically pure or analytically pure. The purity of commercially available reaction materials
88 was maintained above 95%. The reactions were monitored by thin-layer chromatography (TLC)
89 silica gel glass plates (Yantai Jiangyou Silica Gel Development Co., Ltd., Yantai, China). ^{1}H

90 and ^{13}C NMR spectra were obtained on a nuclear magnetic resonance 600/400 spectrometer
91 (Varian Inc., Palo Alto, CA) in $CDCl_3$ or DMSO-d_6 with tetramethylsilane (TMS).
92 High-resolution mass spectrometry (HRMS) of the target compounds were performed on an
93 Agilent 6224 TOF LC/MS (Agilent Technologies, Santa Clara, CA). the melting points of the
94 compounds were measured on a melting point apparatus model (Büchi model B-545, Flawil,
95 Switzerland), and the temperature was uncorrected.

96 **Molecular Simulation**. The crystal structure of AtHPPD (PDB ID: 1TFZ and 1TG5) was
97 downloaded from the Protein Data Bank. The purified HPPD was obtained by expression of the
98 recombinant Arabidopsis enzyme in *E. coli.*[28] The sequences of 1TFZ and 1TG5 contained 21
99 truncated amino acid residues at the N-terminus in order to express the recombinant
100 Arabidopsis enzyme in *E. coli*. The co-crystal structures of 1TFZ and 1TG5 were all homo
101 dimeric form and their active pockets are highly conserved. The main difference between them
102 was the bound inhibitors. So, we believe whatever we use 1TFZ or 1TG5 will result in the same
103 docking results. Herein, 1TFZ was selected at random for docking study. During molecular
104 docking, the number of amino acid residues was increased by 21 to make it consistent with the
105 wild-type. First, we used SYBYL 7.3 (Tripos Inc., St. Louis, MO) to construct and optimize the
106 tested compounds and used AutoDock Tools (ADT) to prepare the protein and ligand structures.
107 Generally, the *At*HPPD-DAS645 co-crystal structure (PDB ID: 1TG5) was used as a reference,
108 and the Fe^{2+} center was regarded as the crucial activity site.[29-33] Applying the GOLD version
109 3.0 docking program, all docking runs were carried out using the default settings of the
110 program on a population size of 100 individuals with a selection pressure of 1.1. We chose the
111 best combination mode with high docking scores to analysis the binding mode of the inhibitor

112 in the active pocket.

113 ***At*HPPD Enzymatic Assay and Crystallization of complex *At*HPPD−9bj**. We adopted
114 the same method as we reported previously to express and purify recombinant *At*HPPD
115 (Supporting Information **S2**).[34-36] Using a classical coupled enzyme assay, the half-maximal
116 inhibitory concentration (IC_{50}) values were determined, and the values are shown in **Table s2**
117 **(**Supporting Information **S10)**.[3, 37, 38] We selected compound **9bj** with excellent enzymatic
118 inhibitory activity as a representative to incubate with *At*HPPD and successfully obtained the
119 co-crystal structure (Supporting Information **S3**).

120 **Herbicidal Activity Test.** The broadleaf weeds *Amaranthus retroflexu* (AR), *Eclipta*
121 *prostrata* (EP), *Abutilon juncea* (AJ), *Amaranthus tricolor* (AT), and *Chenopodium album* (CA)
122 and gramineous weeds *Echinochloa crusgalli* (EC), *Setaria faberii* (SF), and *Digitaria*
123 *sanguinalis* (DS) were chosen as the target weeds to evaluate the postemergence herbicide
124 activity of compounds **9aa−9bj** in a greenhouse.[36, 39] We choose pyrasulfotole and mesotrione
125 (Supporting Information **S1**) as the control, and use the same method that we reported early to
126 test the herbicidal activity (Supporting Information **S6**)[36]. After 25 days of treatment, the results
127 of herbicidal activity were evaluated visually with three repetitions per treatment, and the
128 results are shown in **Table s2** and **Table 1**.

129 **Crop Safety Test.** Seven major crops, maize, soybeans, cotton, wheat, rice, canola, and
130 peanuts were chosen as representatives to evaluate the crop selectivity of the target compounds
131 under greenhouse conditions.[2, 34] Using self−formulated mixed soil, the crops were planted in
132 flowerpots (12 cm in diameter) and grown in the greenhouse at 20−25°C. Postemergence crop
133 safety experiments were carried out at the dose of 150 g ai/ha for the tested compounds when

134 the crops reached the three-leaf stage. Crop selectivity was evaluated 25 days after treatment
135 with title compounds **9aj**, **9bi** and **9bj** in triplicate, and the results are shown in **Table 2**.

136 **RESULTS AND DISCUSSION**

137 **Chemistry.** As shown in **Figure 3**, the designed pyrazole−quinazoline-2,4-dione hybrids
138 **9aa−9bh** were synthesized in eight continuous reaction steps. First, the oxidation of
139 5-methyl-2-nitrobenzoic acid **1** was performed with aqueous $KMnO_4$ under alkaline conditions,
140 followed by esterification of the carboxyl groups and reduction of the nitro groups to yield
141 dimethyl 4-aminoisophthalate **4**.[34, 35] Intermediate **4** was refluxed with (un)substituted (R^2)
142 phenyl isocyanates in pyridine to obtain N3-aryl-quinazoline-2,4-diones **5aa−5ba**. Under
143 alkaline conditions, compounds **5aa−5ba** were treated with various alkyl iodides (R^1-I) to
144 prepare quinazoline-2,4-dione derivatives **6aa−6bh**. Then, the ester group was hydrolyzed
145 under acidic conditions to obtain the corresponding key intermediate acids **7aa−7bh**.
146 Subsequently, using 2-chloro-1-methylpyridin-1-ium iodide (CMPI) as the condensing agent,
147 Et_3N and 1,3-dimethyl-1*H*-pyrazol-5-ol in one pot resulted in intermediate enol esters **8aa−8bh**.
148 After simple processing, the final title compounds **9aa−9bh** were obtained by the Fries
149 Rearrangement.

150 In another synthesis scheme, we chose 2-methyl-6-nitrobenzoic acid as the starting
151 material to synthesize the designed compounds **9bi−9bj (Figure 4)**. First, we used the common
152 reaction conditions of esterification, nitro reduction and aromatic ring bromination to obtain the
153 intermediate (IV). Then, the same methods for synthesizing intermediates **5aa−5ba** and
154 **6aa−6bh** were used to prepare the crucial intermediate (VI). In contrast, we used palladium
155 catalysis and 4,5-bis(diphenylphosphino)-9,9-dimethylxanthene (xantphos) as the ligand under

156 a CO atmosphere to synthesize title compounds (**9bi**−**9bj**) from the aryl bromides (VI) directly.
157 The chemical structures of all the synthesized target compounds were confirmed by ^{1}H NMR
158 and ^{13}C NMR spectroscopy and HRMS (Supporting Information **S7**−**S9**). Since the hydrogen
159 on the hydroxyl group is particularly active, it is very easy to exchange with D from the
160 solvents DMSO-d_6 or $CDCl_3$ and difficult to detect by NMR. Therefore, we do not detect the
161 hydrogen of the hydroxyl group. Furthermore, a transparent crystal of compound **9bi** was
162 obtained directly from $CDCl_3$ and confirmed by single-crystal X-ray diffraction (**Figure 5**). The
163 crystallographic data have been submitted to the Cambridge Crystallographic Data Centre
164 (CCDC ID: 1970427).

165 ***At*HPPD Inhibition and Structure−Activity Relationships (SAR)**. During the
166 investigation of the binding mode of **9aa** (**Figure 2**), the N3 position was surrounded by
167 hydrophobic amino acid residues (Leu427 and Leu368), and a similar observation was found at
168 the N1 position (Met335). The results indicated that a hydrophobic substituent at the N1
169 position or N3 position would be beneficial for inhibitory activity in vitro. To verify the
170 molecular simulation results, we first introduced a hydrophobic aromatic ring at the N3 position
171 and a methyl at the N1 position to synthesize compound **9aa**. The half-maximal inhibitory
172 concentration (IC_{50}) of compound **9aa** against *At*HPPD reached 0.514 μM, which was two
173 times better than that of the control agent pyrasulfotole (IC_{50} = 1.359 μM) but worse than that
174 of mesotrione (IC_{50} = 0.226 μM). Furthermore, we added the hydrophobic methyl group to the
175 N3 benzene ring to synthesize compound **9ab** (R^1 = CH_3, R^2 = 2-CH_3). The generated
176 compound **9ab** (IC_{50} = 0.428 μM) showed better inhibitory activity against *At*HPPD than parent
177 **9aa**. The in vitro activity was consistent with the experimental results of molecular docking.

178 Hence, we tried to optimize the substituents around the N1 position (R^1) and N3 phenyl ring
179 (R^2) of quinazoline-2,4-dione.

180 Based on the molecular skeleton of compound **9ab**, compounds **9ac**−**9ai** were obtained by
181 introducing a hydrophobic alkyl chain into the N1 position (R^1), and their *At*HPPD inhibition
182 parameters are listed in **Table s2** For compounds with ethyl (**9ac**) or *n*-propyl (**9ad**), the
183 *At*HPPD-inhibiting activities were further improved in comparison with compound **9ab**.
184 Remarkably, attaching an unsaturated alkyl chain to the N1 position in the corresponding
185 compounds **9ag** (R^1 = allyl) and **9ah** (R^1 = propargyl) also showed better inhibitory potency
186 compared with compound **9ab**. However, when we introduced the *n*-butyl (**9ae**), *iso*-butyl (**9af**)
187 or benzyl (**9ai**) groups to the N1 position, the inhibitory activity of these compounds gradually
188 decreased as the spatial distribution of the substituents increased.

189 Simultaneously, keeping the N1 position as a methyl group, a single substituent was
190 introduced to the N3 phenyl ring as R^2. The in-vitro activity results of compounds (**9aj**−**9at**) are
191 shown in **Table s2**. Generally, a substituent at the *para* position of the N3 phenyl ring could
192 improve the inhibitory effect better than a substituent in the *ortho* position; i.e., 4-CH_2CH_3 (**9ao**,
193 IC_{50} = 0.177 μM) > 2-CH_2CH_3 (**9aj**, IC_{50} = 0.401 μM) and 4-OCF_3 (**9as,** IC_{50} = 0.235 μM) >
194 2-OCF_3 (**9am**, IC_{50} = 0.284 μM). In particular, at the *para* position, the inhibitory activity was
195 enhanced with increasing steric hindrance of the substituent. The order of the inhibition activity
196 was 4-OPh (**9at**, IC_{50} = 0.130 μM) > 4-CH_2CH_3 (**9ao**, IC_{50} = 0.177 μM) > 4-CH_3 (**9an**, IC_{50} =
197 0.361 μM). In addition, regardless of whether the substituent was in the *ortho* or *para* position
198 of the N3 phenyl ring, the inhibitory activity against *At*HPPD increased with enhancement of
199 the electron−withdrawing ability of the substituent; i.e., 2-OCF_3 > 2-OCH_3 (**9al**) > 2-CH_3 (**9ab**),

200 and 4-CF_3 (**9aq**) > 4-OCF_3 (**9as**) > 4-OCH_3 (**9ar**) > 4-CH_3 (**9an**). A special case was the
201 compound containing a strong electron−withdrawing group, 4-NO_2 (**9ap**, IC_{50} = 0.139 μM),
202 which displayed lower inhibitory activity than **9aq** (4-CF_3, IC_{50} = 0.075 μM).

203 In recent years, other specific nonbonded contacts have been reported, e.g., halogen bonds,
204 CH-π, and cation-π interactions.[40-43] The halogen bond (XB), an emerging noncovalent
205 intermolecular interaction analogous to the hydrogen bond (HB), has made significant
206 contributions to the molecular recognition in protein-ligand interactions.[44] Thus, keeping N1
207 position as a methyl group, we synthesized monohalogenated derivatives on the N3 benzene
208 ring (R^2: F, Cl, Br) and investigated their bioactivity in vitro (**9au**−**9bc**). At the *ortho* or *meta*
209 position of the N3 phenyl ring, introducing a chloro substituent was helpful to increase the
210 inhibitory activity compared to fluoro or bromo substituents. However, the enzyme inhibition
211 activity was discrepant for the same substituent at the different positions of the N3 phenyl ring.
212 The trend of those compounds was 2-F > 3-F > 4-F, 3-Cl > 2-Cl > 4-Cl and 4-Br > 2-Br > 3-Br.
213 Therefore, there may be a certain interaction among fluorine, chlorine or bromine and the
214 enzyme active pocket that has not yet been demonstrated.

215 In addition, we evaluated the inhibitory activities of these compounds with multiple
216 substitutions (di, tri) on the N3 phenyl ring (**9bd**−**9bh**, **Table s2**). The compound with the
217 diethyl substitution (**9be**) was better than that the compound with the dimethyl substitution
218 (**9bd**). Moreover, an electron−withdrawing group at the *para* position of the N3 phenyl ring
219 also resulted in increasing inhibitory activity (R^2: 2-Cl-4-NO_2 > 2,4-di-Cl). When we added a
220 tri-methyl group (**9bf**) to the phenyl ring, the inhibitory activity was better than that of the
221 dimethyl derivative (**9bd**), but it was similar to that of the monomethyl derivative (**9ab**)

222 (2,4,6-tri-CH_3 ≈ 2-CH_3 > 2,6-di-CH_3). In addition, keeping the R^2 group as a single methyl or
223 chlorine on the *ortho* position of the N3 phenyl ring, we synthesized compounds **9bi**−**9bj** with a
224 methyl at the 5 position of quinazoline-2,4-dione. The in vitro test results confirmed that
225 compounds **9bi** and **9bj** were better than compounds **9ab** and **9ax**, respectively. In particular,
226 compound **9bj** showed high *At*HPPD inhibitory activity with an IC_{50} value of 84 nM, which
227 was approximately 2.7 times higher than that of mesotrione (IC_{50} = 226 nM). Furthermore, we
228 carried out molecular docking. When compounds **9ab** and **9bi** maintain a similar binding
229 conformation (**Figure 6A** and **6B**), we observed that the binding model of **9bi** was in a
230 suboptimal conformation according to its docking score ranking and binding free energy, which
231 was only -3.113 kcal/mol. However, after optimizing the conformation (**Figure 6C)**, the very
232 significant change was that the orientation of the N3 benzene ring was deflected. Moreover, the
233 binding free energy of **9bi** was reduced to -9.859 kcal/mol, which was better than **9ab** (ΔH =
234 -5.861 kcal/mol). Thus, all the results suggested that a methyl group at the 5-position of the
235 quinazoline-2, 4-dione fragment would be essential for improving biological activity.

236 **Crystal Structure of *At*HPPD−9bj Complex (PDB ID: 6LGT)**. Using the method we
237 reported earlier, we successfully obtained the co-crystal structure of *At*HPPD−**9bj**.[15, 25, 45] The
238 structure of the *At*HPPD−**9bj** complex was solved by molecular replacement, and the resolution
239 of the complex was refined to 1.75 Å (Supporting Information **S4** and **S5**). As shown in **Figure**
240 **7A**, the interaction between the inhibitor and protein in the co-crystal structure of *At*HPPD−**9bj**
241 was similar to that of the reported commercial HPPD inhibitor, which contained a bidentate
242 chelating interaction with the metal ion, and a π-π stacking interaction with Phe381 and Phe424.
243 In contrast, from the omit map of **9bj** (**Figure 7B**), due to the free rotation of the C−N bond, the

244 *o*-chlorophenyl at the N3 position showed double conformations. In addition, two water
245 molecules are observed near the inhibitor in **Figure 7C**. The distance from water (a) to water (b)
246 is 2.8 Å, and water (a) made a potential hydrogen bond with the nitrogen of Asn282. Water (b)
247 is 3.4 Å away from the carbonyl group of the inhibitor and made other potential hydrogen
248 bonds with the nitrogen atoms of Gln293 and Gln307, which are fully conserved in all known
249 HPPD proteins. To gain insight into the differences in binding modes between **9bj** and the
250 commercial herbicide in the active pocket, we superimposed this complex structure onto the
251 complex structure of *At*HPPD-mesotrione (**Figure 7D**). In general, in addition to common
252 interactions, the nitro group of mesotrione and the methyl group on the 5-position of
253 quinazoline-2,4-dione maintain almost the same orientation. The biggest difference was that the
254 terminal *o*-chlorophenyl fragment was near the entrance of the active pocket and was
255 surrounded by hydrophobic amino acids (such as Met335, Leu368, Leu427, Phe424, Phe392,
256 and Phe381; Supporting Information **S4**). Thus, the introduction of hydrophobic substituents at
257 the N3 position was beneficial for improving the biological activity of the inhibitor.

258 **Herbicidal Activity.** We tested the postemergence herbicidal activities of all synthetic
259 compounds at a dose of 150 g ai/ha. The weeds produced the same unique bleaching symptoms
260 after dealing with our synthetic compounds and controls. The herbicidal activity results are
261 shown in **Table s2**. For the N1 position, methyl−substituted compounds **9aa** and **9ab** showed
262 more than 50% of the control effect for all the tested weeds. The other compounds with
263 unsaturated alkyl chains also displayed more than 50% inhibition for most of the tested weeds.
264 However, when the alkyl chain had more than three carbon atoms, as in compounds **9ae, 9af**
265 and **9ai**, there was obvious herbicidal activity under the same test conditions. Thus, at the N1

266 position, the methyl group would be the best for improving the herbicide activity.

267 On the N3 phenyl ring, some compounds (**9aj**–**9at**) with mono substitutions displayed a
268 complete control effect for one of the tested weeds (*Abutilon juncea* or *Amaranthus retroflexus*)
269 and showed a better control effect on *Setaria faberii* (SF) than the control. In particular, the
270 compound **9aj** (2-CH_2CH_3) can completely control the three types of broadleaf weeds (AJ, AR
271 and EP), maintaining a control effect of more than 70% for the tested grass weeds. In addition,
272 the compounds with mono substitutions at the *ortho* position of the N3 phenyl ring displayed
273 better weed control effects than substitutions at the *para* position. For example, 2-CH_3 > 4-CH_3,
274 2-OCH_3 > 4-OCH_3 and 2-OCF_3 > 4-OCF_3. In addition, compounds that contained strong
275 electron-withdrawing groups or phenoxy groups at the *para* position of the N3 phenyl ring had
276 better inhibitory activity against *At*HPPD, but they exhibited poor herbicidal activities.
277 Moreover, for compounds with monohalogenated substitution, a similar trend was observed,
278 and the herbicidal activity of the *ortho*-substituted compounds led to an obvious increase in
279 potency when compared to the *para*- or *meta*-substituted derivatives. For example, compounds
280 **9au** (2-F), **9ax** (2-Cl) and **9ba** (2-Br), had more than 50% control effects on the tested weeds.
281 The control potential of these compounds displayed a better control effect on *Setaria faberii*
282 (SF) compared with the control. Furthermore, compounds with multiple substitutions on the N3
283 phenyl ring (**9bd**–**9bh**) did not improve herbicidal activity. More importantly, compounds **9bi**
284 and **9bj** with a methyl at the 5-position of quinazoline-2,4-dione displayed excellent control
285 efficiency for all the tested weeds and was significantly improved compared to their
286 corresponding parent compounds **9ab** and **9ax**, respectively. Thus, substituting the 5-position of
287 the quinazoline-2, 4-dione fragment would be essential for improving herbicide activity.

288 Due to the excellent level of control weed activity, compounds **9aj**, **9bi**, and **9bj** were
289 chosen for further testing at lower doses (**Table 1**). When the dosage was lowered from 120 g
290 ai/ha to 30 g ai/ha, the herbicidal activities of compounds **9aj** and **9bj** also decreased. However,
291 the control weed potency of compound **9bi** was maintained at more than 70%, except for
292 *Abutilon juncea* (AJ). In our work, the in vitro activity of some compounds was better than that
293 of the control, but they did not show obvious control effects on the tested weeds. As we know,
294 in plants, the process of absorption, conduction, and metabolism is very important for
295 herbicides to exert their effects.[46, 47] These factors were very likely the cause of the differences
296 in activity observed in vitro and in vivo.

297 **Crop Selectivity.** The crop safety of compounds **9aj**, **9bi** and **9bj** was evaluated at the
298 dose of 150 g ai/ha (**Table 2)**. The results indicated that compound **9aj** showed no injury to
299 cotton or peanuts. However, obvious injury symptoms appeared in cotton after using
300 mesotrione in the greenhouse. Additionally, compound **9bi** displayed good tolerance to corn.
301 Compound **9bj** had an excellent herbicidal effect, but the phytotoxicity was also obvious to the
302 seven crops under the tested conditions. Thus, these three compounds have potential application
303 prospects in the future.

304 In summary, using a ring−expansion strategy, a series of novel quinazoline−2,4-dione
305 derivatives were designed and synthesized. The two synthetic routes were chosen to prepare
306 title compounds (**9aa−9bj**). Of the two routes, one was catalysed by palladium under a CO
307 atmosphere to prepare the designed compounds **9bi−9bj**. From the SAR analysis, at the N1
308 position (R^1), a methyl would be the best group for improving herbicide activity. For the N3
309 position, on one hand, an electron-withdrawing group on the N3 phenyl ring was beneficial for

310 improving enzyme inhibition activity, but it was not good for enhancing herbicidal activity. On
311 the other hand, the *pata*-substituted derivatives were better for in vitro inhibition activity than
312 the *ortho*-substituted derivatives. However, the *ortho*-substituted derivatives displayed better
313 herbicidal activity. In addition, the co-crystal structure of *At*HPPD−**9bj** was obtained at a
314 resolution of 1.75 Å and confirmed the mechanism of action at the atomic level. Furthermore,
315 under greenhouse conditions, many compounds displayed excellent postemergence herbicidal
316 activities against one of the tested weeds at the dose of 150 g ai/ha. In particular, compound **9aj**
317 was selective for cotton and peanuts, which was promising for development as a selective
318 postemergence HPPD-target herbicide. Compound **9bi** provided an excellent weed control
319 effect and showed better safety to corn at the dose of 150 g ai/ha. In addition, compound **9bj**
320 has superior herbicidal activity, but its crop safety needs further improvement. Thus,
321 pyrazole−quinazoline-2,4-dione derivatives will be very promising for the development of
322 novel HPPD inhibitors.
323

324 **Supporting Information**

325 The Supporting Information is available free of charge on the ACS Publications website; **S1**.
326 The structure of commercial HPPD herbicides; **S2**. Protein expression and purification; **S3**.
327 Crystallization and structure determination of complex *At*HPPD−**9bj** (PDB ID: 6LGT); **S4**. The
328 overall co-crystal structure of *At*HPPD-**9bj** (PDB ID: 6LGT); **S5**. Data collection and
329 refinement statistics of the crystal structure of *At*HPPD−**9bj** (PDB ID: 6LGT); **S6**. The testing
330 method of herbicide activity; **S7**. Synthetic method and physical data of compounds **9aa**−**9bh**;
331 **S8**. Synthetic method and physical data of compounds **9bi**−**9bj**; **S9**. Spectra of representative

compounds **9aa−9bj**; and **S10**. Chemical Structures and Bioactivity of Compounds **9aa−9bj**.

Acknowledgments

This work was supported by the National Key Research and Development Program of China (2018YFD0200100) and the National Natural Science Foundation of China (Nos. 21837001, 21672079 and 21772058).

Notes

The authors declare no competing financial interest.

REFERENCES

(1) Hao, G. F.; Tan, Y.; Xu, W. F.; Cao, R. J.; Xi, Z.; Yang, G. F., Understanding resistance mechanism of protoporphyrinogen oxidase-inhibiting herbicides: insights from computational mutation scanning and site-directed mutagenesis. *J. Agric. Food Chem* **2014**, *62*, 7209-7215.

(2) Wang, D. W.; Li, Q.; Wen, K.; Ismail, I.; Liu, D. D.; Niu, C. W.; Wen, X.; Yang, G. F.; Xi, Z., Synthesis and Herbicidal Activity of Pyrido[2,3-d]pyrimidine-2,4-dione-Benzoxazinone Hybrids as Protoporphyrinogen Oxidase Inhibitors. *J. Agric. Food Chem* **2017**, *65*, 5278-5286.

(3) Ndikuryayo, F.; Moosavi, B.; Yang, W. C.; Yang, G. F., 4-Hydroxyphenylpyruvate dioxygenase inhibitors: from chemical biology to agrochemicals. *J. Agric. Food Chem* **2017**, *65*, 8523-8537.

(4) He, B.; Wang, D. W.; Yang, W. C.; Chen, Q.; Yang, G. F., Advances in Research on 4-Hydroxyphenylpyruvate Dioxygenase (HPPD) Structure and Pyrazole-Containing Herbicides.

354 *Chin. J. Org. Chem* **2017**, *37*, 2895-2904.

355 (5) Ahrens, H.; Lange, G.; Muller, T.; Rosinger, C.; Willms, L.; van Almsick, A.,
356 4-Hydroxyphenylpyruvate dioxygenase inhibitors in combination with safeners: solutions for
357 modern and sustainable agriculture. *Angew. Chem.* **2013**, *52*, 9388-9398.

358 (6) Fu, Y.; Wang, K.; Wang, P.; Kang, J. X.; Gao, S.; Zhao, L. X.; Ye, F., Design, Synthesis,
359 and Herbicidal Activity Evaluation of Novel Aryl-Naphthyl Methanone Derivatives. *Front.*
360 *Chem.* **2019**, *7*, 1-10.

361 (7) Crouch, N. P.; Adlington, R. M.; Baldwin, J. E.; Lee, M. H.; MacKinnon, C. H., A
362 mechanistic rationalisation for the substrate specificity of recombinant mammalian
363 4-hydroxyphenylpyruvate dioxygenase (4-HPPD). *Tetrahedron* **1997**, *53*, 6993-7010.

364 (8) Borowski, T.; Bassan, A.; Siegbahn, P. E., 4-Hydroxyphenylpyruvate dioxygenase: a hybrid
365 density functional study of the catalytic reaction mechanism. *Biochemistry* **2004**, *43*,
366 12331-12342.

367 (9) Fritze, I. M.; Linden, L.; Freigang, J.; Auerbach, G.; Huber, R.; Steinbacher, S., The crystal
368 structures of Zea mays and Arabidopsis 4-hydroxyphenylpyruvate dioxygenase. *Plant Physiol*
369 **2004**, *134*, 1388-1400.

370 (10) Brownlee, J. M.; Johnson-Winters, K.; Harrison, D. H.; Moran, G. R., Structure of the
371 ferrous form of (4-hydroxyphenyl)pyruvate dioxygenase from Streptomyces avermitilis in
372 complex with the therapeutic herbicide, NTBC. *Biochemistry* **2004**, *43*, 6370-6377.

373 (11) Moran, G. R., 4-Hydroxyphenylpyruvate dioxygenase. *Arch. Biochem. Biophys* **2005**, *433*,
374 117-128.

375 (12) Xu, K.; Racine, F.; He, Z.; Juneau, P., Impacts of hydroxyphenylpyruvate dioxygenase

376 (HPPD) inhibitor (mesotrione) on photosynthetic processes in Chlamydomonas reinhardtii.
377 *Environ Pollut* **2019**, *244*, 295-303.
378 (13) Wojcik, A.; Broclawik, E.; Siegbahn, P. E.; Lundberg, M.; Moran, G.; Borowski, T., Role
379 of substrate positioning in the catalytic reaction of 4-hydroxyphenylpyruvate dioxygenase-A
380 QM/MM Study. *J. Am. Chem. Soc* **2014**, *136*, 14472-14485.
381 (14) Santucci, A.; Bernardini, G.; Braconi, D.; Petricci, E.; Manetti, F.,
382 4-Hydroxyphenylpyruvate dioxygenase and its inhibition in plants and animals: small
383 molecules as herbicides and agents for the treatment of human inherited diseases. *J. Med. Chem*
384 **2017**, *60*, 4101-4125.
385 (15) Lin, H. Y.; Yang, J. F.; Wang, D. W.; Hao, G. F.; Dong, J. Q.; Wang, Y. X.; Yang, W. C.;
386 Wu, J. W.; Zhan, C. G.; Yang, G. F., Molecular insights into the mechanism of
387 4-hydroxyphenylpyruvate dioxygenase inhibition: enzyme kinetics, X-ray crystallography and
388 computational simulations. *FEBS J* **2019**, *286*, 975-990.
389 (16) Fu, Y.; Zhang, S. Q.; Liu, Y. X.; Wang, J. Y.; Gao, S.; Zhao, L. X.; Ye, F., Design,
390 synthesis, SAR and molecular docking of novel green niacin-triketone HPPD inhibitor. *Ind.*
391 *Crops Prod.* **2019**, *137*, 566-575.
392 (17) Fu, Y.; Zhang, D.; Zhang, S.-Q.; Liu, Y.-X.; Guo, Y.-Y.; Wang, M.-X.; Gao, S.; Zhao,
393 L.-X.; Ye, F., Discovery of N-Aroyl Diketone/Triketone Derivatives as Novel
394 4-Hydroxyphenylpyruvate Dioxygenase Inhibiting-Based Herbicides. *J. Agric. Food Chem*
395 **2019**, *67*, 11839-11847.
396 (18) Yamaoka, K.; Nakagawa, M.; Ishida, M., Hydrolysis of the Rice Herbicide Pyrazolate in
397 Aqueous Solutions. *J. Pestic. Sci.* **1987**, *12*, 209-212.

398 (19) Kaundun, S. S.; Hutchings, S. J.; Dale, R. P.; Howell, A.; Morris, J. A.; Kramer, V. C.;
399 Shivrain, V. K.; McIndoe, E., Mechanism of resistance to mesotrione in an Amaranthus
400 tuberculatus population from Nebraska, USA. *PLoS One* **2017**, *12*, e0180095.
401 (20) Grossmann, K.; Ehrhardt, T., On the mechanism of action and selectivity of the corn
402 herbicide topramezone: a new inhibitor of 4-hydroxyphenylpyruvate dioxygenase. *Pest Manag.*
403 *Sci.* **2007**, *63*, 429-439.
404 (21) Zhang, J.; Zheng, L.; Jäck, O.; Yan, D.; Zhang, Z.; Gerhards, R.; Ni, H., Efficacy of four
405 post-emergence herbicides applied at reduced doses on weeds in summer maize (Zea mays L.)
406 fields in North China Plain. *Crop Prot.* **2013**, *52*, 26-32.
407 (22) Liu, X.; Xiao, Y.; Li, J. Q.; Fu, B.; Qin, Z., 1,1-Diaryl compounds as important bioactive
408 module in pesticides. *Molecular Diversity* **2019**, *23*, 809-820.
409 (23) Kohrt, J. R.; Sprague, C. L., Response of a Multiple-Resistant Palmer Amaranth
410 (Amaranthus palmeri) Population to Four HPPD-Inhibiting Herbicides Applied Alone and with
411 Atrazine. *Weed Sci.* **2017**, *65*, 534-545.
412 (24) Maeda, H.; Murata, K.; Sakuma, N.; Takei, S.; Yamazaki, A.; Karim, M. R.; Kawata, M.;
413 Hirose, S.; Kawagishi-Kobayashi, M.; Taniguchi, Y.; Suzuki, S.; Sekino, K.; Ohshima, M.;
414 Kato, H.; Yoshida, H.; Tozawa, Y., A rice gene that confers broad-spectrum resistance to
415 beta-triketone herbicides. *Science* **2019**, *365*, 393-396.
416 (25) He, B.; Dong, J.; Lin, H. Y.; Wang, M. Y.; Li, X. K.; Zheng, B. F.; Chen, Q.; Hao, G. F.;
417 Yang, W. C.; Yang, G. F., Pyrazole-Isoindoline-1,3-dione Hybrid: A Promising Scaffold for
418 4-Hydroxyphenylpyruvate Dioxygenase Inhibitors. *J Agric Food Chem* **2019**, *67*, 10844-10852.
419 (26) Zhao, P. L.; Wang, L.; Zhu, X. L.; Huang, X.; Zhan, C. G.; Wu, J. W.; Yang, G. F.,

420 Subnanomolar inhibitor of cytochrome bc1 complex designed by optimizing interaction with
421 conformationally flexible residues. *J Am Chem Soc* **2010**, *132*, 185-194.
422 (27) Hao, G. F.; Wang, F.; Li, H.; Zhu, X. L.; Yang, W. C.; Huang, L. S.; Wu, J. W.; Berry, E.
423 A.; Yang, G. F., Computational discovery of picomolar Q(o) site inhibitors of cytochrome bc1
424 complex. *J Am Chem Soc* **2012**, *134*, 11168-11176.
425 (28) Yang, C.; Pflugrath, J. W.; Camper, D. L.; Foster, M. L.; Pernich, D. J.; Walsh, T. A.,
426 Structural basis for herbicidal inhibitor selectivity revealed by comparison of crystal structures
427 of plant and mammalian 4-hydroxyphenylpyruvate dioxygenases. *Biochemistry* **2004**, *43*,
428 10414-10423.
429 (29) Yang, C.; Pflugrath, J. W.; Camper, D. L.; Foster, M. L.; Pernich, D. J.; Walsh, T. A.,
430 Structural Basis for Herbicidal Inhibitor Selectivity Revealed by Comparison of Crystal
431 Structures of Plant and Mammalian 4-Hydroxyphenylpyruvate Dioxygenases. *Biochemistry*
432 **2000**, *43*, 10414-10423.
433 (30) Spiliotopoulos, D.; Caflisch, A., Fragment-based in silico screening of bromodomain
434 ligands. *Drug Discovery Today: Technol.* **2016**, *19*, 81-90.
435 (31) Chen, Q.; Zhu, X. L.; Jiang, L. L.; Liu, Z. M.; Yang, G. F., Synthesis, antifungal activity
436 and CoMFA analysis of novel 1,2,4-triazolo[1,5-a]pyrimidine derivatives. *Eur. J. Med. Chem*
437 **2008**, *43*, 595-603.
438 (32) Fu, Q.; Cai, P. P.; Cheng, L.; Zhong, L. K.; Tan, C. X.; Shen, Z. H.; Han, L.; Xu, T. M.;
439 Liu, X. H., Synthesis and herbicidal activity of novel pyrazole aromatic ketone analogs as
440 HPPD inhibitor. *Pest Manag Sci* **2020**, *76*, 868-879.
441 (33) Fu, Y.; Liu, Y. X.; Yi, K. H.; Li, M. Q.; Li, J. Z.; Ye, F., Quantitative Structure Activity

442 Relationship Studies and Molecular Dynamics Simulations of
443 2-(Aryloxyacetyl)cyclohexane-1,3-Diones Derivatives as 4-Hydroxyphenylpyruvate
444 Dioxygenase Inhibitors. *Front. Chem.* **2019**, *7*, 556.
445 (34) Wang, D. W.; Lin, H. Y.; Cao, R. J.; Yang, S. G.; Chen, T.; He, B.; Chen, Q.; Yang, W. C.;
446 Yang, G. F., Synthesis and bioactivity studies of triketone-containing quinazoline-2,4-dione
447 derivatives. *Acta Chim. Sinica* **2015**, *73*, 29-35.
448 (35) Wang, D. W.; Lin, H. Y.; Cao, R. J.; Ming, Z. Z.; Chen, T.; Hao, G. F.; Yang, W. C.; Yang,
449 G. F., Design, synthesis and herbicidal activity of novel quinazoline-2,4-diones as
450 4-hydroxyphenylpyruvate dioxygenase inhibitors. *Pest Manage. Sci* **2015**, *71*, 1122-1132.
451 (36) Wang, D. W.; Lin, H. Y.; Cao, R. J.; Chen, T.; Wu, F. X.; Hao, G. F.; Chen, Q.; Yang, W.
452 C.; Yang, G. F., Synthesis and herbicidal activity of triketone-quinoline hybrids as novel
453 4-hydroxyphenylpyruvate dioxygenase inhibitors. *J. Agric. Food Chem.* **2015**, *63*, 5587-5596.
454 (37) Meazza, G.; Scheffler, B. E.; Tellez, M. R.; Rimando, A. M.; Romagni, J. G.; Duke, S. O.;
455 Nanayakkara, D.; Khan, I. A.; Abourashed, E. A.; Dayan, F. E., The inhibitory activity of
456 natural products on plant p-hydroxyphenylpyruvate dioxygenase. *Phytochemistry* **2002**, *60*,
457 281-288.
458 (38) Schmidt, S. R.; Muller, C. R.; Kress, W., Murine liver homogentisate 1,2-dioxygenase.
459 Purification to homogeneity and novel biochemical properties. *Eur. J. Biochem* **1995**, *228*,
460 425-430.
461 (39) Zuo, Y.; Wu, Q. Y.; Su, S. W.; Niu, C. W.; Xi, Z.; Yang, G. F., Synthesis, Herbicidal
462 Activity, and QSAR of Novel N-Benzothiazolyl- pyrimidine-2,4-diones as Protoporphyrinogen
463 Oxidase Inhibitors. *J. Agric. Food Chem* **2016**, *64*, 552-562.

464 (40) Umezawa, Y.; Nishio, M., CH/π hydrogen bonds as evidenced in the substrate specificity
465 of acetylcholine esterase. *Biopolymers* **2005**, *79*, 248-258.
466 (41) Lu, Y.; Wang, Y.; Xu, Z.; Yan, X.; Luo, X.; Jiang, H.; Zhu, W., C-X...H contacts in
467 biomolecular systems: how they contribute to protein-ligand binding affinity. *J. Phys. Chem. B*
468 **2009**, *113*, 12615-12621.
469 (42) Zou, W. S.; Lin, S.; Li, J. Y.; Wei, H. Q.; Zhang, X. Q.; Shen, D. X.; Qiao, J. Q.; Lian, H.
470 Z.; Xie, D. Q.; Ge, X., Mechanism and application of halogen bond induced fluorescence
471 enhancement and iodine molecule cleavage in solution. *New J. Chem.* **2015**, *39*, 262-272.
472 (43) Xiu, X.; Puskar, N. L.; Shanata, J. A.; Lester, H. A.; Dougherty, D. A., Nicotine binding to
473 brain receptors requires a strong cation-pi interaction. *Nature* **2009**, *458*, 534-538.
474 (44) Metrangolo, P.; Resnati, G., Chemistry. Halogen versus hydrogen. *Science* **2008**, *321*,
475 918-919.
476 (45) Lin, H. Y.; Chen, X.; Chen, J. N.; Wang, D. W.; Wu, F. X.; Lin, S. Y.; Zhan, C. G.; Wu, J.
477 W.; Yang, W. C.; Yang, G. F., Crystal structure of 4-hydroxyphenylpyruvate dioxygenase in
478 complex with substrate reveals a new starting point for herbicide discovery. *Research* **2019**,
479 *2019*, 1-11.
480 (46) Miao, Z.; Scott Obach, R., Chapter 10 Alcohols and Phenols: Absorption, Distribution,
481 Metabolism and Excretion. In *Metabolism, Pharmacokinetics and Toxicity of Functional*
482 *Groups: Impact of Chemical Building Blocks on ADMET*, The Royal Society of Chemistry:
483 2010; pp 460-485.
484 (47) Hwang, K. H.; Lim, J. S.; Kim, S. H.; Jeon, M. S.; Lee, D. G.; Chung, K. H.; Koo, S. J.;
485 Kim, J. H., In vivo absorption, distribution, excretion, and metabolism of a new herbicide,

methiozolin, in rats following oral administration. *J. Agric. Food Chem.* **2013**, *61*, 9285-9292.

508 **Figure captions:**

509 **Figure 1.** Chemical structures of some commercial pyrazole HPPD herbicides.

510 **Figure 2.** The design strategy of compounds **9aa−9bj**. The binding free energy of **s1**, $\triangle H_{s1}$ =
511 -6.322 kcal/mol. The binding free energy of **9ab,** $\triangle H_{9aa}$ = -8.349 kcal/mol.

512 **Figure 3.** Synthetic route of the title compounds **9aa−9bh**. Reagents and conditions: (a)
513 $KMnO_4$, KOH, 80°C; (b) CH_3OH, H_2SO_4, reflux; (c) H_2, 10% Pd/C, rt; (d) (un)substituted
514 penylisocyanates, pyridine, 100°C; (e) alkyl iodide , Cs_2CO_3, DMF, rt; (f) HOAc, H_2SO_4, H_2O,
515 100°C; (g) 2-chloro-1-methylpyridin-1-ium iodide (CMPI), Et_3N, DCM,
516 1,3-dimethyl-1H-pyrazol-5-ol, rt; (h) acetone cyanohydrin, Et_3N, acetonitrile, 25°C.

517 **Figure 4.** Synthetic route of the title compounds **9bi−9bj**. Reagents and conditions: (a) CH_3OH,
518 H_2SO_4, reflux; (b) H_2, 10% Pd/C, ethyl acetate, rt; (c) NBS, 1,2-dichloroethane, 0°C; (d)
519 substituted penylisocyanates, pyridine, 100°C; (e) iodomethane, Cs_2CO_3, DMF, rt; (f) Xantphos,
520 $PdCl_2$, Et_3N, K_2CO_3, CO, DMF, 100°C.

521 **Figure 5.** X-ray crystal structure of compound **9bi.**

522 **Figure 6.** The molecular docking model of compounds **9ab** and **9bi** with *At*HPPD (PDB No.
523 1TFZ), where green represents the inhibitor molecule and blue represents the amino acid
524 residue at the active pocket. (A) Binding free energy of **9ab**, ΔH = -5.861 kcal/mol; (B)
525 Binding free energy of **9bi**, non-optimal combined conformation, ΔH = -3.123 kcal/mol; and (C)
526 Binding free energy of **9bi**, optimal combined conformation, ΔH = -9.857 kcal/mol.

527 **Figure 7.** Co-crystal structure of *At*HPPD−**9bj** (green) and the structural comparison with
528 *At*HPPD-mesotrione (purple). Inhibitors and the key surrounding residues of the active pocket
529 are highlighted as sticks. The chelation interactions and hydrogen bonds are indicated with

black dashed lines. (A) The binding mode of compound **9bj** with *At*HPPD and its interaction with adjacent amino acid residues. (B) 2Fo-Fc map (contoured at 1.0 σ) of compound **9bj**. (C) Water molecules mediating the hydrogen bonding network in the *At*HPPD−**9bj** active pocket. (D) The superposition of the binding modes of **9bj** and mesotrione in *At*HPPD.

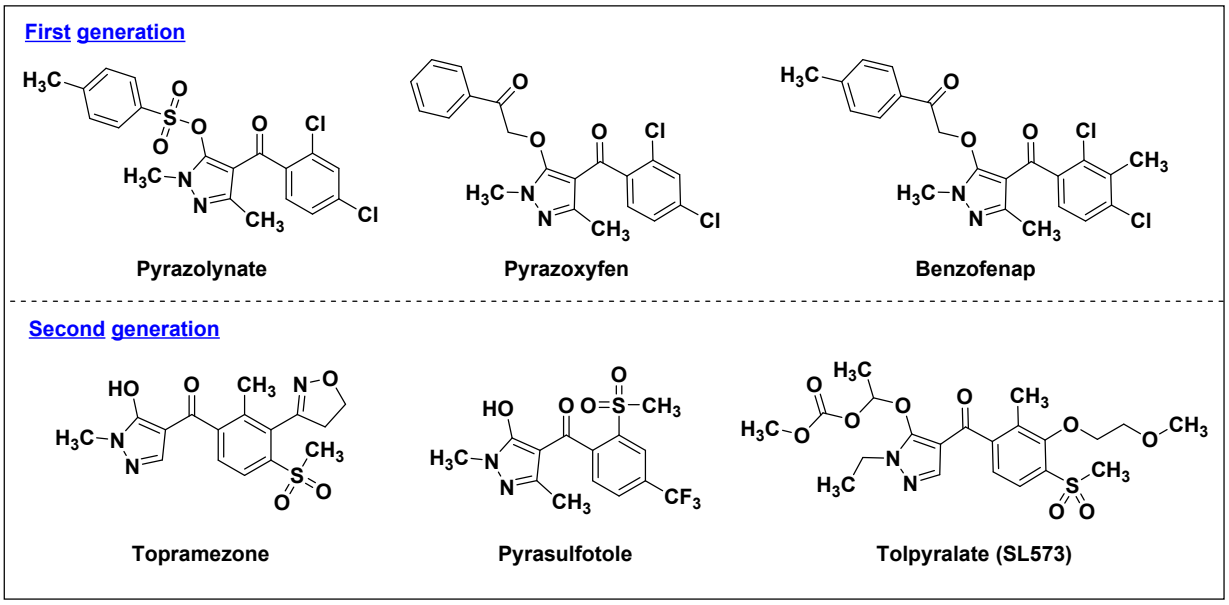

548

549 **Figure 1**

550

551

552

553

554

555

556

557

558

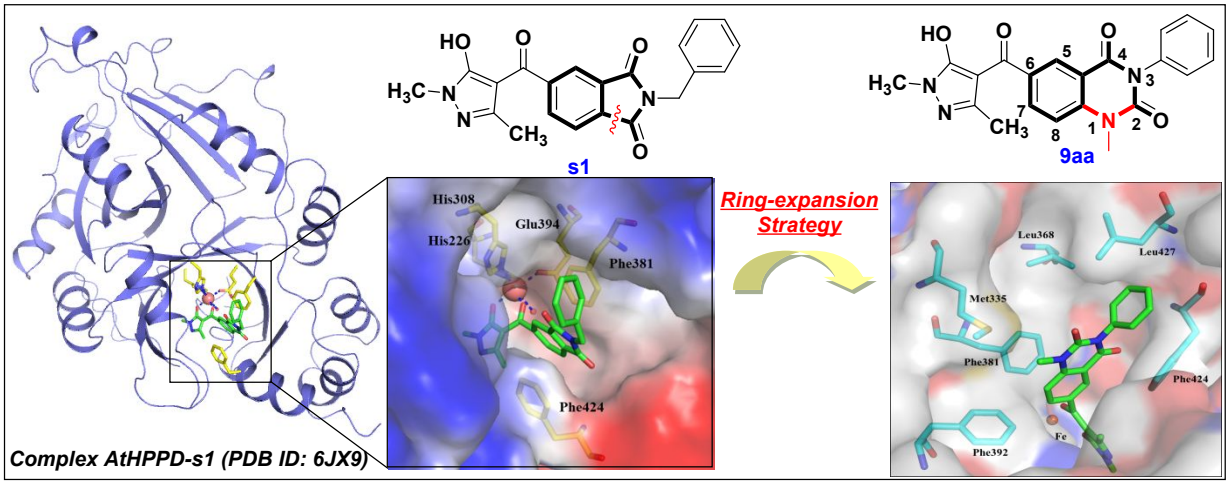
HO
O
O
O
H_3C–N
N
N
CH_3
s1
HO
O
O
H_3C–N
N
CH_3
6
5
4
N
3
7
8
1
N
2
O
9aa
Complex AtHPPD-s1 (PDB ID: 6JX9)
His308
Glu394
His226
Phe381
Phe424
Ring-expansion
Strategy
Leu368
Leu427
Met335
Phe381
Phe424
Fe
Phe392

Figure 2

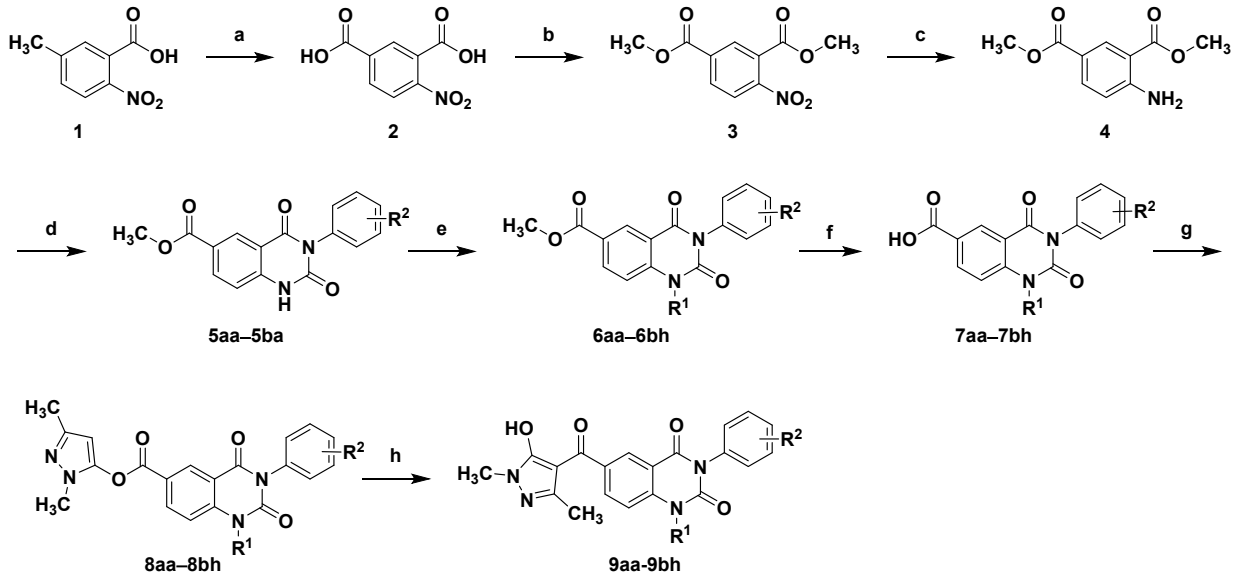

Figure 3

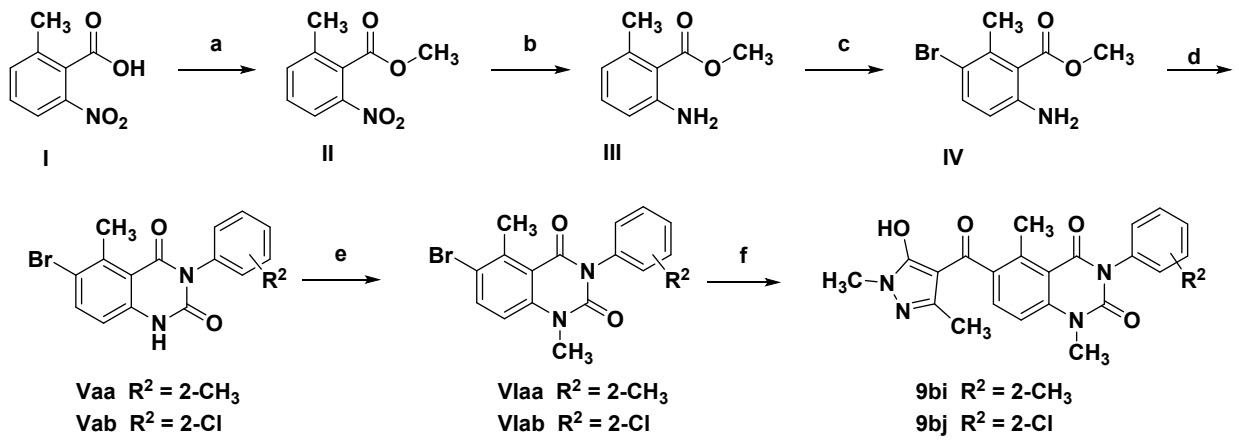

Vaa R^2 = 2-CH_3
Vab R^2 = 2-Cl

VIaa R^2 = 2-CH_3
VIab R^2 = 2-Cl

9bi R^2 = 2-CH_3
9bj R^2 = 2-Cl

Figure 4

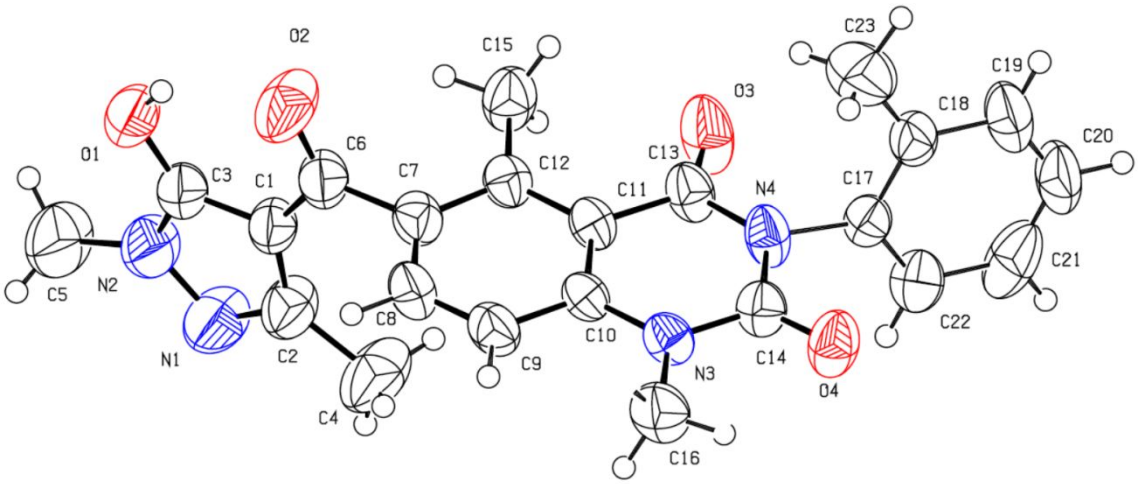
O2
C15
C23
C19
O3
C18
C20
O1
C6
C13
C3
C1
C7
C12
C11
N4
C17
C5
N2
C21
C8
C10
C22
N1
C2
C9
N3
C14
O4
C4
C16

Figure 5

616

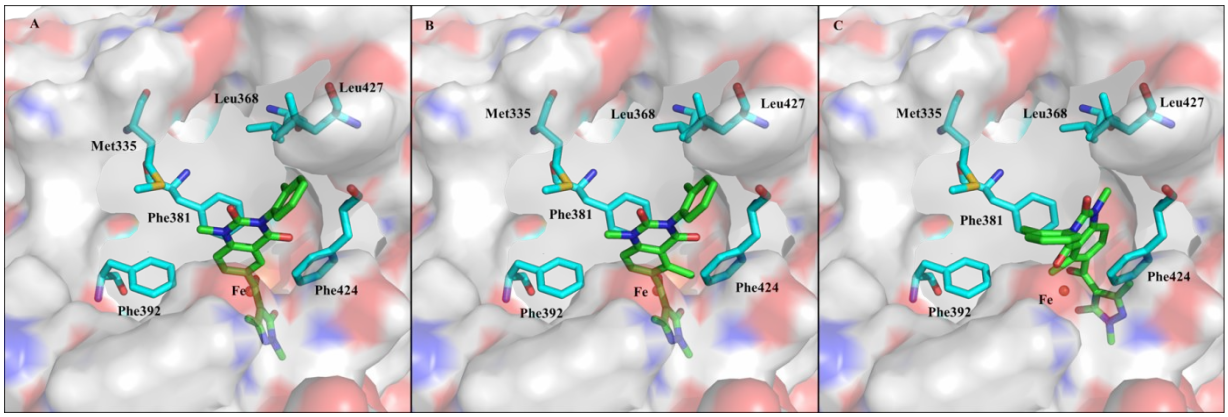

617 **Figure 6**

618

619

620

621

622

623

624

625

626

627

628

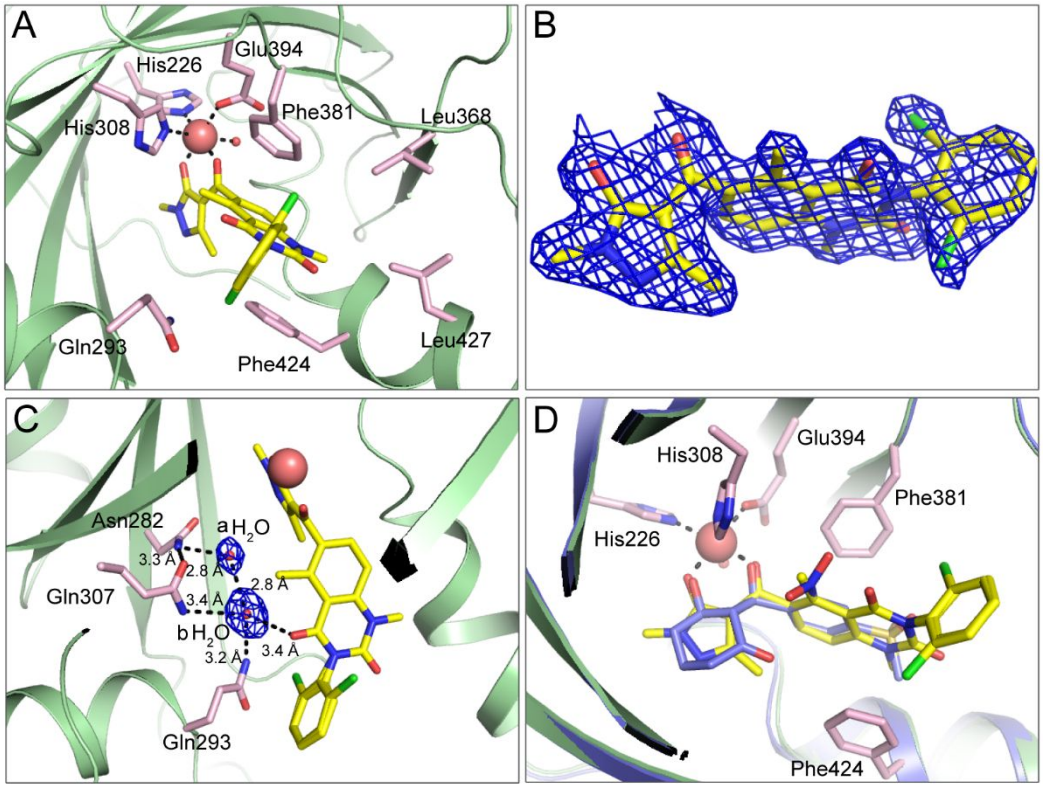

Figure 7

643 **Table 1. Postemergence Herbicidal Activity of Compounds 9aj, 9bi and 9bj**

Compd.	Dose (g ai/ha)	% Inhibition					
		SF[a]	EC	DS	AT	CA	AJ
9aj	30	B[b]	C	E	E	E	E
	60	B	B	E	D	E	E
	120	B	C	C	B	D	A
9bi	30	A	A	--[c]	C	B	D
	60	A	A	--	C	A	D
	120	A	A	--	A	A	A
9bj	30	D	C	D	C	E	C
	60	C	B	D	C	E	C
	120	A	A	B	A	A	A
Mesotrione	30	G	E	E	E	D	E
	60	G	C	C	B	B	A
	120	E	A	A	A	A	A

[a]Abbreviations: SF, Setaria faberii; EC, Echinochloa crus-galli; DS, Digitaria sanguinalis; AT, Amaranthus tricolor; CA, Chenopodium album; AJ, Abutilon juncea; [b]Rating scale of inhibition percent in relation to the untreated control: A = 100%; B ≥ 90%; C, ≥ 70%; D, ≥ 50%; E, ≥ 20%; F, ≥ 10%; G, 0-10%; [c]Dotted line indicates untested.

644

645

646

647

648

649

650

651

652

653

654

655

656 **Table 2. Postemergence Crop Selectivity of Compounds 9aj, 9bi and 9bj**

Compd.	Dose (g ai/ha)	% Injury						
		corn	soybean	cotton	wheat	peanut	rice	canola
9aj	150	E[a]	E	G	F	G	E	E
9bi	150	G	C	D	E	D	C	A
9bj	150	E	D	E	E	E	D	A
Mesotrione	150	G	E	E	G	--[b]	E	F

[a]Rating scale of inhibition percent in relation to the untreated control: A = 100%; B ≥ 90%; C, ≥ 70%; D, ≥ 50%; E, ≥ 20%; F, ≥ 10%; G, 0-10%; [b] Dotted line indicates untested.

657

658

659

660

661

662

663

664

665

666

667

668

669

670

671

672

673 **Graphic for table of contents**

674 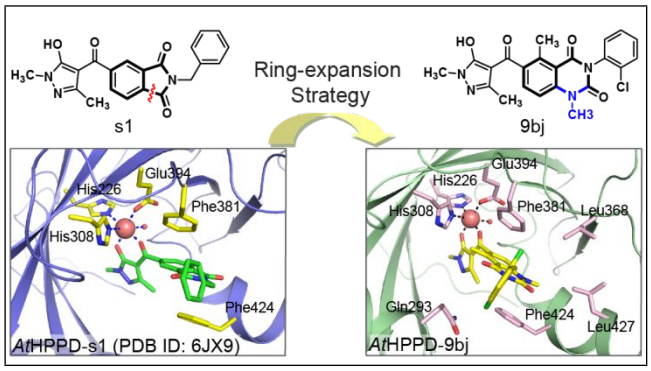

675

676

677

678

679

680

681

682

683